Metallic Polypthalocyanine Catalyst for Selective CO_2 Electroreduction

Raaf Alqahtany

Abdulrahman Allangawi

raaf.alqahtany@kaust.edu.sa

abdulrahman.allangawi@kaust.edu.sa

Abstract

Electrochemical CO_2 reduction offers a promising pathway for converting carbon dioxide into valuable chemicals and fuels using renewable electricity. However, achieving high product selectivity while maintaining efficient catalytic performance remains a major challenge. Here we explore metal polyphthalocyanines as tunable electrocatalysts for selective CO_2 electroreduction by examining the effects of metal composition, capping-agent modification, catalyst loading and polymeric architecture. Bimetallic Co–Ni polyphthalocyanines showed composition-dependent reduction pathways, with $Co_{3.1}Ni_1PPc$ enabling deeper CO_2 reduction toward methanol, while monometallic NiPPc strongly favored CO formation. Capping-agent modification with tetraphenylphthalic anhydride (TPPA) further enhanced NiPPc performance, with NiPPc-p achieving essentially quantitative CO Faradaic efficiency from -0.90 to -1.20 V versus RHE with no detectable H_2 formation. At the optimized loading of 0.4 mg cm^{-2}, NiPPc-p reached an average current density of approximately 43 mA cm^{-2} at -1.20 V while maintaining a stable current response. Compared with molecular NiPc, NiPPc-p showed higher selectivity, current response and stability, highlighting the benefit of the polymeric framework. NiPPc-p also showed highly competitive performance compared with reported Ni-phthalocyanine-based catalysts, combining essentially quantitative CO selectivity with high current density. These findings demonstrate the potential of metal polyphthalocyanines as tunable electrocatalysts for controlling CO_2 reduction pathways and selectivity, providing a basis for developing efficient CO_2 conversion systems toward value-added chemicals.

Introduction

Electrochemical reduction of carbon dioxide (CO_2) has emerged as a promising approach for carbon conversion, as it can utilize clean electrical energy under mild conditions to convert CO_2 into valuable chemical products [1,2]. The CO_2 reduction reaction (CO_2RR) proceeds through multiple electron- and proton-transfer pathways, producing valuable products ranging from the two-electron reduction product CO, an important chemical feedstock, to more deeply reduced products such as methanol, an important chemical fuel [3,4]. However, the high thermodynamic stability and chemical inertness of CO_2, together with the competing hydrogen evolution reaction (HER), make the control of the reduction pathway challenging [5]. Therefore, the development of efficient electrocatalysts that combine high product selectivity and electrochemical activity remains essential for effective CO_2 electrochemical conversion [6].

Noble metals, particularly Au and Ag, exhibit high activity and selectivity toward electrochemical CO_2 reduction; however, their high cost and limited abundance constrain their large-scale application [7]. This has driven increasing interest in earth-abundant transition metals such as Ni and Co, owing to their lower cost, abundance, and tunable catalytic properties [8,9]. Their CO_2RR activity and selectivity, however, are strongly governed by the local coordination and electronic environment of the metal centers, making control of this environment essential [10]. Molecular catalysts provide such control through structurally well-defined ligand frameworks [11]. Among these, metal phthalocyanines (MPcs) have attracted considerable interest for CO_2RR owing to their well-defined $M–N_4$ active sites, with CoPc and NiPc showing promising CO_2 reduction activity [12]. More recently, extending these molecular units into conjugated metal polyphthalocyanine (MPPc) frameworks has emerged as a strategy to further enhance electrocatalytic performance through improved electronic communication and charge transport while preserving the $M–N_4$ active sites [13]. The polymeric architecture also provides opportunities for further tuning through metal composition and framework modification [14]. Despite substantial progress with Co-based polyphthalocyanines, Ni-centered systems remain comparatively less explored for CO_2RR, with reported NiPc catalysts often relying on conductive supports such as carbon nanotubes, leaving the catalytic potential of the conjugated Ni polyphthalocyanine framework itself less established [15-17].

Herein, we investigate Ni-based polyphthalocyanine frameworks as tunable electrocatalysts for CO_2 reduction by systematically examining the effects of metal composition, capping-agent modification, catalyst loading, and polymeric architecture. Bimetallic Co-Ni polyphthalocyanines with different metal ratios were first explored to determine whether interactions between Co and Ni centers could invoke deeper CO_2 reduction pathways. The behavior of monometallic NiPPc was subsequently established, followed by capping-agent modification using tetraphenylphthalic anhydride (TPPA) to improve the catalytic response of the Ni-centered framework. Optimization of the catalyst loading and comparison

with molecular NiPc further enabled the contributions of electrode composition and the polymeric environment to be distinguished. The optimized NiPPc-p catalyst achieved essentially quantitative CO Faradaic efficiency with no detectable H_2 formation while sustaining high and stable current densities, demonstrating the potential of polyphthalocyanine framework engineering for highly selective CO_2-to-CO electrocatalysis.

Methodology

Catalyst Synthesis

Synthesis of NiPPc. NiPPc was synthesized by thoroughly grinding NH_4Cl (1.00 g), urea (4.10 g), phthalic anhydride (PA; 0.30 g), pyromellitic dianhydride (PMDA; 1.74 g), $NiCl_2$ (0.66 g), and $(NH_4)_6Mo_7O_{24}{\cdot}4H_2O$ (0.025 g) in an agate mortar. The resulting homogeneous mixture was transferred to a 250 mL ceramic crucible and heated in a muffle furnace at 220 °C for 3 h at a heating rate of 5 °C min^{-1}.

Synthesis of Co_xNi_yPPc. The bimetallic $Co_{3.1}Ni_1PPc$ and Co_5Ni_1PPc polymers were synthesized following the procedure described for NiPPc, except that $NiCl_2$ was replaced by the corresponding mixtures of $CoCl_2$ and $NiCl_2$. $Co_{3.1}Ni_1PPc$ was prepared using $CoCl_2$ (0.50 g) and $NiCl_2$ (0.16 g), whereas Co_5Ni_1PPc was prepared using $CoCl_2$ (0.55 g) and $NiCl_2$ (0.11 g). All other precursor quantities and synthesis conditions were maintained unchanged.

Synthesis of NiPPc-p. NiPPc-p was synthesized following the procedure described for NiPPc, with PA (0.30 g) replaced by an equal mass of tetraphenylphthalic anhydride (TPPA; 0.30 g). All other precursor quantities and synthesis conditions were maintained unchanged.

Synthesis of NiPc. Molecular NiPc was synthesized following the procedure described for NiPPc, except that PMDA was omitted and the amount of PA was increased to 3.02 g. All other precursor quantities and synthesis conditions were maintained unchanged.

Purification of the Synthesized Catalysts. Following synthesis, the obtained products were allowed to cool to room temperature, ground in an agate mortar, and transferred into 50 mL centrifuge tubes. The samples were sequentially washed with distilled water, ethanol, and N,N-dimethylformamide (DMF). In each washing step, the samples were centrifuged at 12,000 rpm (15,284 ×g) for 20 min, and each washing step was repeated twice. The purified powder catalysts were finally dried under vacuum at 80 °C overnight.

Catalyst Characterization

Powder X-ray diffraction (PXRD) patterns of the synthesized catalysts were recorded using a Bruker X-ray diffractometer equipped with a LYNXEYE XE-T detector and Cu Kα radiation (λ = 1.5418 Å), operated at 40 kV and 40 mA. Diffraction patterns were collected over a 2θ range of 5-70° with a step size of approximately 0.02° and a counting time of 0.25 s per step. FTIR spectra were recorded using a Thermo Scientific FTIR spectrometer equipped with a Smart iTR attenuated total reflectance (ATR) accessory over the wavenumber range of approximately 4000-500 cm^{-1}.

Electrode Preparation

Catalyst Ink Preparation. Of each catalyst powder, catalyst inks were prepared by separately dispersing 7.5 mg of each catalyst in 15 mL of N-methyl-2-pyrrolidone (NMP) to obtain a concentration of 0.5 mg mL^{-1}. The resulting suspensions were probe-sonicated for 1 h at 675 W using a pulsed sequence of 3 s ON and 1 s OFF while maintained in an ice bath to minimize heating.

Drop-Casting of Catalyst Ink. The catalyst inks were drop-cast onto PTFE-treated carbon paper (22BB) over a defined geometric area of approximately 0.5 × 1.0 cm^2. Prior to catalyst deposition, the designated electrode area was treated with 80 µL of ethanol and allowed to dry. Catalyst loadings of 0.2, 0.4, and 0.6 mg cm^{-2} were obtained by sequentially depositing four 50 µL, five 80 µL, and ten 60 µL aliquots of the corresponding catalyst ink, respectively. Each aliquot was dried under an infrared lamp prior to subsequent deposition. Following catalyst deposition, 50 µL of 4 mg mL^{-1} Nafion in ethanol solution was applied to the catalyst-coated electrode and dried under an infrared lamp.

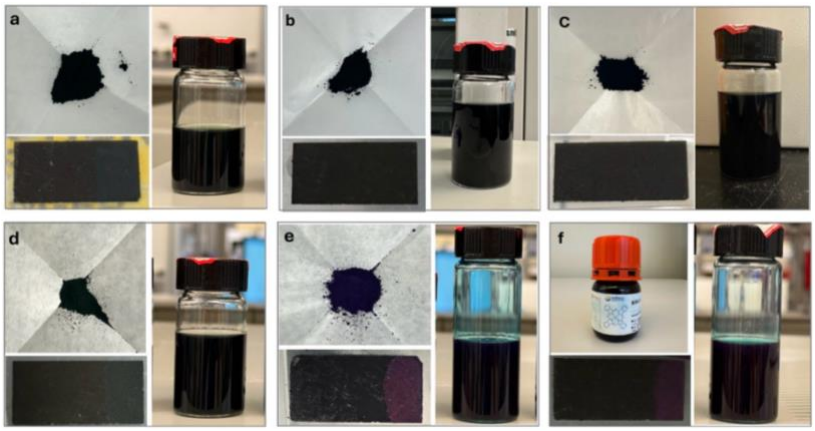


Figure 1. Catalyst powders, inks and coated electrodes of **(a)** NiPPc, **(b)** $Co_{3.1}Ni_1PPc$, **(c)** Co_5Ni_1PPc, **(d)** NiPPc-p, **(e)** NiPc and (**f**) NiPc commercial

Electrochemical Measurements

Electrochemical CO_2 reduction measurements were performed in an H-type cell using catalyst-coated carbon paper as the working electrode, an Ag/AgCl electrode as the reference electrode, and a platinum plate as the counter electrode. The cathodic and anodic compartments were separated by an ion-exchange membrane, and each compartment contained 50 mL of 0.5 M $KHCO_3$ electrolyte. Prior to electrolysis, CO_2 was continuously bubbled through the cathodic electrolyte at a flow rate of 20 sccm for at least 20 min under continuous magnetic stirring to obtain a CO_2-saturated electrolyte. Chronoamperometric electrolysis was performed using a Bio-Logic VMP3 potentiostat at applied potentials of -0.80, -0.90, -1.00, -1.10, and -1.20 V versus the reversible hydrogen electrode (RHE), with each potential applied for 30 min. Potentials applied

experimentally against the Ag/AgCl reference electrode were converted to the RHE scale according to: $E_{RHE} = E_{Ag/AgCl} + E^{ref}_{Ag/AgCl} + 0.0591\ pH$ where $E_{Ag/AgCl}$ is the applied potential versus the Ag/AgCl reference electrode and $E^{ref}_{Ag/AgCl}$ is the potential of the Ag/AgCl reference electrode relative to the standard hydrogen electrode. Under the experimental conditions employed, the conversion corresponded to an offset of approximately +0.63 V (e.g., -1.43 V vs Ag/AgCl corresponded to -0.80 V vs RHE). Fresh electrolyte was used for each applied potential.

Product Quantification

Gas Chromatography. During electrolysis, the outlet gas was continuously directed to a gas chromatograph (GC), where gaseous products were automatically analyzed twice during each experiment. H_2 and CO were quantified from their corresponding chromatographic peak areas using previously established GC calibration factors. The resulting gas concentrations, together with the gas flow rate and electrolysis current, were used to determine the Faradaic efficiencies of the gaseous products.

^{1}H NMR Analysis. Liquid-phase products were analyzed by ^{1}H NMR spectroscopy. After each electrolysis experiment, 2.0 mL of the collected electrolyte was mixed with 200 µL of D_2O and 40 µL of DMSO. After thorough mixing, three 560 µL aliquots of the resulting solution were transferred into separate NMR tubes for analysis. The same procedure was repeated for the electrolyte collected at each applied potential. The ^{1}H NMR spectra were acquired using a standard ^{1}H NMR experiment with D_2O as the deuterated solvent. Liquid products were identified from their characteristic ^{1}H NMR resonances and quantified relative to DMSO as the internal standard.

Faradaic Efficiency Calculation

The Faradaic efficiency (FE) of each product was calculated as the fraction of the total charge transferred toward formation of the corresponding product:

$$FE_i(\%) = \frac{z_i n_i F}{Q} \times 100$$

where z_i is the number of electrons transferred per molecule of product i, n_i is the amount of product formed, F is the Faraday constant (96,485 C mol^{-1}), and Q is the total charge passed during electrolysis. For the gaseous products H_2 and CO, two electrons per molecule were used in the FE calculations. The Faradaic efficiencies of liquid products were calculated using the corresponding electron-transfer numbers determined from their respective reduction reactions.

Results and Discussion

Effect of Bimetallic Co-Ni Polyphthalocyanines on CO_2 Reduction

Initially, cobalt-nickel bimetallic polyphthalocyanines were explored to determine whether synergy between the Co and Ni centers could enhance CO_2 reduction

and invoke the formation of deeper carbon reduction products, such as methanol. Accordingly, $Co_{3}Ni_{1}$PPc and $Co_{5}Ni_{1}$PPc were synthesized by varying the relative ratios of the cobalt and nickel precursors (Fig. 1b,c). The formation of the targeted Co-Ni polyphthalocyanines was evaluated by PXRD and FTIR spectroscopy. The PXRD patterns of $Co_{3}Ni_{1}$PPc and $Co_{5}Ni_{1}$PPc exhibited similar crystalline characteristics and closely aligned diffraction profiles (Fig. 2). FTIR analysis showed characteristic functional-group vibrations associated with the phthalocyanine framework, with both bimetallic compositions displaying comparable spectral features (Fig. 3). Furthermore, the agreement of both bimetallic polyphthalocyanines with previously reported CoPPc reference materials from the research group in both PXRD and FTIR supports the successful formation of the desired Co-Ni polyphthalocyanine catalysts.

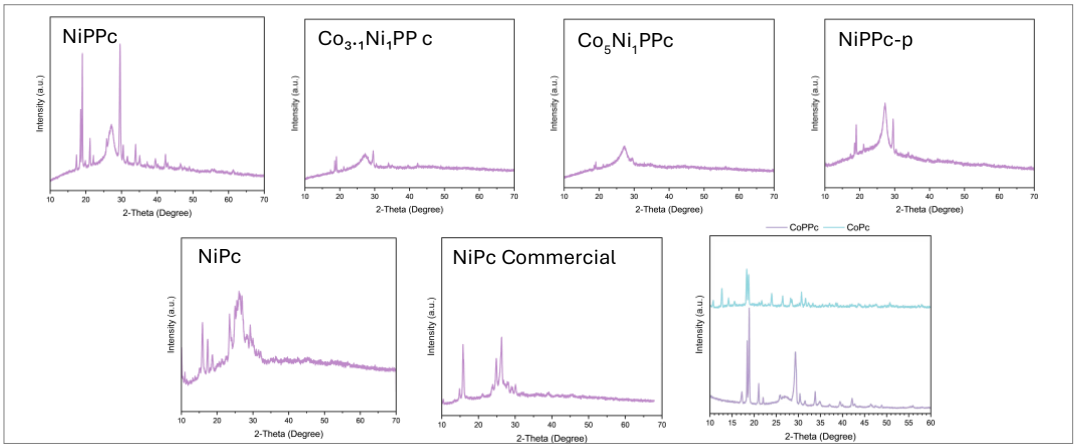


Figure 2 | PXRD characterization of the synthesized phthalocyanine catalysts. PXRD spectra of NiPPc, $Co_{3}Ni_{1}$PPc, $Co_{5}Ni_{1}$PPc, NiPPc-p, and NiPc, together with CoPPc and CoPc reference spectra for comparison.

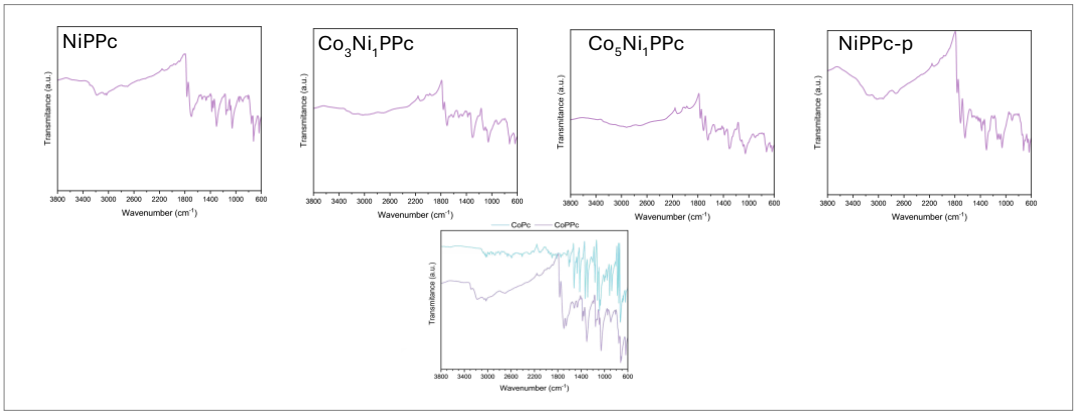


Figure 3 | FTIR characterization of the synthesized phthalocyanine catalysts. FTIR spectra of NiPPc, $Co_{3}Ni_{1}$PPc, $Co_{5}Ni_{1}$PPc, NiPPc-p, together with CoPPc and CoPc reference spectra for comparison.

The electrocatalytic CO_2 reduction performance of $Co_{3.1}Ni_1PPc$ was evaluated at a catalyst loading of 0.4 mg cm^{-2} over the potential range from -0.80 to -1.20 V versus RHE. As shown in Fig. 4a, the catalyst exhibited pronounced selectivity toward CO_2 reduction over the competing hydrogen evolution reaction (HER), with CO constituting the predominant product over most of the investigated potential range. Notably, the product distribution evolved at more negative potentials, where methanol emerged at -1.10 and -1.20 V versus RHE. The formation of methanol, which proceeds through a six-electron CO_2 reduction pathway compared with the two-electron reduction to CO, indicates that the Co-Ni bimetallic system can invoke deeper carbon reduction beyond CO formation with limited competition from HER.

The chronoamperometric profiles showed substantial current densities throughout the 30 min electrolysis experiments, further demonstrating the electrochemical activity of $Co_{3.1}Ni_1PPc$ (Fig. 4b). Lower current densities were observed at -1.10 and -1.20 V versus RHE, which may be associated with electrode degradation or experimental variability during testing. Nevertheless, the overall current response, together with the product distribution, demonstrates the ability of the bimetallic catalyst to sustain CO_2 reduction while accessing both CO and deeper reduction products.

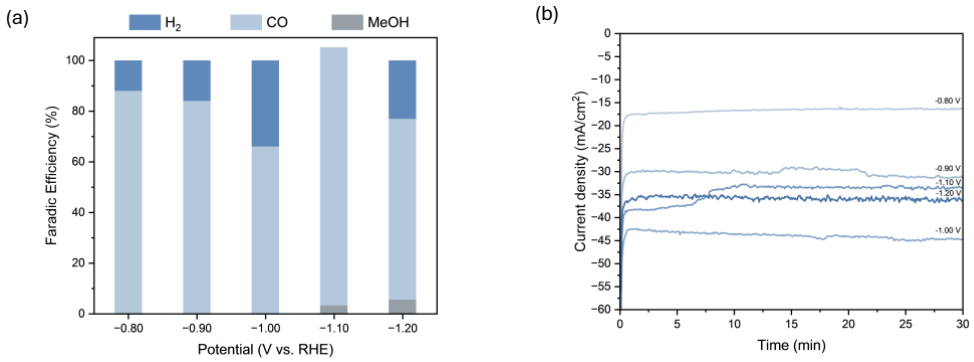


Figure 4 | CO_2RR activity and selectivity of $Co_{3.1}Ni_1PPc$. (a) Product Faradaic efficiencies and (b) chronoamperometric profiles at 0.4 mg cm^{-2}.

To further examine the influence of the relative Co-Ni composition, Co_5Ni_1PPc was evaluated under the same electrochemical conditions. CO was observed as the carbon-reduction product across the investigated potential range, without detectable methanol formation (Fig. 5a). Nevertheless, Co_5Ni_1PPc exhibited substantial current densities, indicating considerable overall electrochemical activity (Fig. 5b). The difference in product distribution between the two bimetallic compositions indicates that altering the relative Co and Ni content affects the accessible CO_2 reduction pathways within the polyphthalocyanine system.

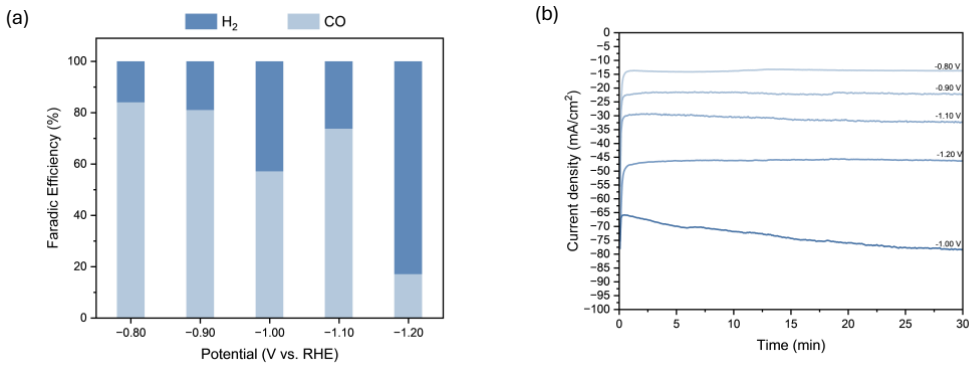


Figure 5 | CO_2RR activity and selectivity of Co_5Ni_1PPc. (a) Product Faradaic efficiencies and (b) chronoamperometric profiles at 0.4 mg cm^{-2}.

Effect of Monometallic Ni Polyphthalocyanine on CO_2 Reduction

Monometallic NiPPc was subsequently investigated as a reference to distinguish the behavior of the Ni-centered polyphthalocyanine from that of the bimetallic systems (Fig. 1a). PXRD and FTIR characterization showed the targeted crystalline characteristics and characteristic functional-group vibrations of the polyphthalocyanine framework, respectively (Figs. 2 and 3). The observed features were consistent with the corresponding CoPPc reference, supporting the successful formation of the NiPPc framework.

The electrocatalytic performance of NiPPc was similarly evaluated at a catalyst loading of 0.4 mg cm^{-2}, enabling direct comparison with the bimetallic systems. Remarkably, the monometallic NiPPc reference emerged as the most selective system toward CO formation among the catalysts investigated at this stage (Fig. 6a). At -0.80 V versus RHE, CO formation competed with HER; however, moving toward more negative potentials induced a pronounced shift toward CO_2 reduction. Between -0.90 and -1.10 V, NiPPc achieved nearly quantitative CO Faradaic efficiency with no detectable H_2, and CO remained strongly favored at -1.20 V with only a minor HER contribution. This pronounced preference for the two-electron CO_2-to-CO pathway distinguishes NiPPc from the broader product selectivity observed for the bimetallic systems.

Furthermore, the selective CO production was accompanied by high current densities throughout the 30 min chronoamperometric measurements (Fig. 6b), demonstrating that the strong selectivity was sustained at considerable electrochemical activity. Although some reduction in current stability was observed at more negative potentials, the overall catalytic response identified NiPPc as a particularly promising system for selective CO_2-to-CO conversion.

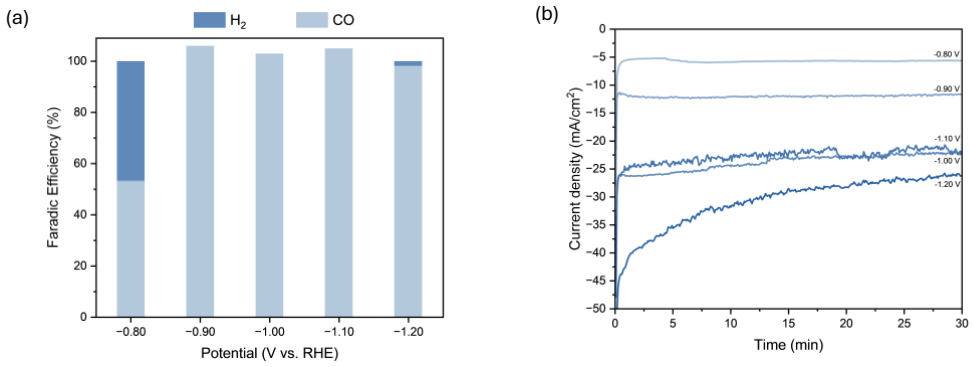


Figure 6 | CO_2RR activity and selectivity of NiPPc. (a) Product Faradaic efficiencies and (b) chronoamperometric profiles at 0.4 mg cm^{-2}.

Effect of Capping Agent and Catalyst-Loading Optimization of NiPPc

NiPPc-p was subsequently synthesized using TPPA as an alternative capping agent (Fig. 1d), based on its reported potential to promote exfoliation of the polyphthalocyanine framework [18], together with previous observations within the research group. PXRD and FTIR characterization of NiPPc-p showed crystalline and functional-group characteristics comparable to those of NiPPc (Figs. 2 and 3), supporting the successful formation of the modified polyphthalocyanine framework. More significantly, electrochemical evaluation at 0.4 mg cm^{-2} revealed a substantial enhancement in the overall catalytic performance (Fig. 7). NiPPc-p achieved essentially 100% CO Faradaic efficiency from -0.90 to -1.20 V versus RHE, with no detectable H_2 formation across these potentials. This quantitative selectivity represents a particularly significant outcome, demonstrating that the modified Ni-polyphthalocyanine directs electrochemical CO_2 reduction almost exclusively toward the two-electron CO pathway (Fig. 7a). The measured FE values slightly exceeded 100% at some potentials owing to experimental uncertainty associated with product quantification and are therefore considered effectively quantitative.

The chronoamperometric response provided an additional improvement over NiPPc, with the 0.4 mg cm^{-2} NiPPc-p electrode sustaining high and stable current densities throughout the 30 min electrolysis period, reaching an average current density of approximately 43 mA cm^{-2} at -1.20 V versus RHE (Fig. 7b). Thus, the capping-agent modification combined essentially quantitative CO selectivity with improved current stability, establishing NiPPc-p as a highly promising catalyst for selective CO_2-to-CO conversion.

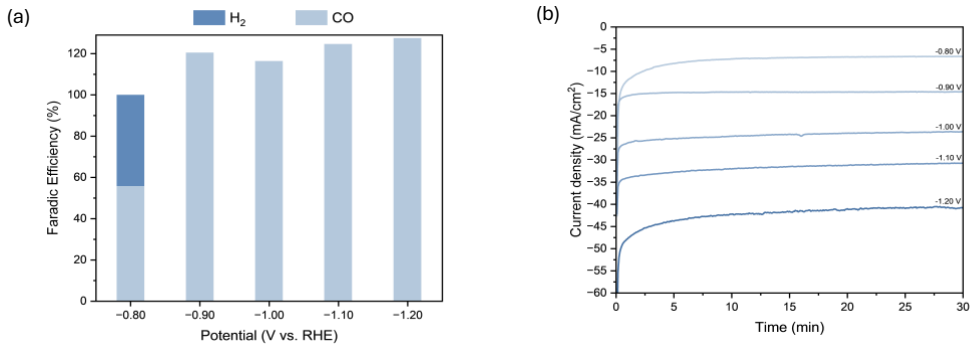


Figure 7 | CO_2RR activity and selectivity of NiPPc-p. (a) Product Faradaic efficiencies and (b) chronoamperometric profiles at 0.4 mg cm^{-2}.

The influence of catalyst loading was subsequently examined by evaluating NiPPc-p at 0.2 and 0.6 mg cm^{-2} alongside the initial 0.4 mg cm^{-2} loading (Fig. 8). Strong CO selectivity was maintained across the investigated loadings; however, clear differences emerged in the chronoamperometric responses. At 0.2 mg cm^{-2}, greater loss of current stability was observed at the most negative potential, whereas the 0.6 mg cm^{-2} electrode showed greater fluctuations in the current profiles. In comparison, 0.4 mg cm^{-2} exhibited the most favorable combination of current density and stability across the investigated potentials (Fig. 8c, f). Overall, these results identify 0.4 mg cm^{-2} as the optimum NiPPc-p loading, combining essentially quantitative CO Faradaic efficiency with the most favorable current response.

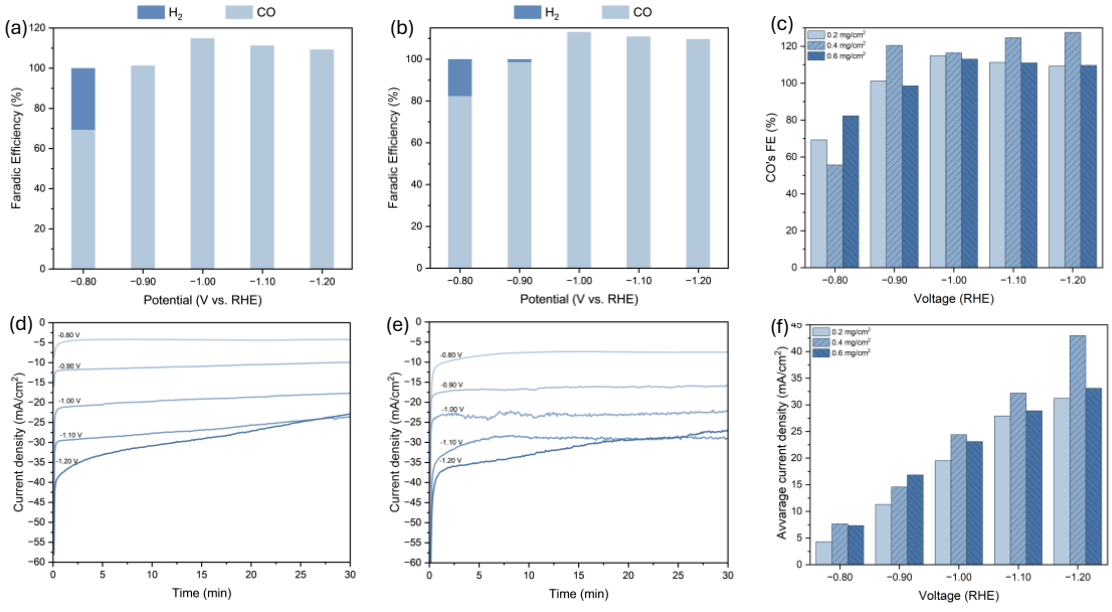


Figure 8 | CO_2RR activity and selectivity of NiPPc-p at different catalyst loadings. Product FE at (a) 0.2 and (b) 0.6 mg cm^{-2}; (c) FE comparison across all loadings; chronoamperometric profiles at (d) 0.2 and (e) 0.6 mg cm^{-2}; and (f) average current-density comparison across all loadings.

Effect of the Polymeric Framework on Ni Active-Site Performance

The effect of the polymeric framework on the catalytic performance of the Ni active sites was examined through comparison with molecular NiPc. Synthesized and commercially available NiPc were therefore evaluated at the same catalyst loading of 0.4 mg cm^{-2} under identical electrochemical conditions (Fig. 1e, f). PXRD characterization of the synthesized NiPc showed the expected structural and characteristic functional-group features, consistent with the corresponding CoPc reference and supporting its successful formation (Fig. 2).
Both molecular NiPc catalysts exhibited appreciable selectivity toward CO formation, particularly at intermediate potentials (Fig. 9a, b). Synthesized NiPc showed higher CO selectivity than commercial NiPc and maintained high Faradaic efficiencies over a broader potential range. In comparison, NiPPc-p maintained essentially quantitative CO Faradaic efficiency at the same potentials with no detectable H_2 formation, demonstrating the more consistent CO_2-to-CO selectivity achieved within the polymeric framework (Fig. 9c).

The distinction was further evident from the chronoamperometric responses (Fig. 9d, e, f). Although both molecular NiPc catalysts were electrochemically active, they exhibited lower current densities and greater current fluctuations at more negative potentials than NiPPc-p. Synthesized NiPc showed an improved current response relative to commercial NiPc yet remained below the current performance and stability achieved by NiPPc-p. Together, the selectivity and current responses demonstrate the catalytic advantage of the polymeric NiPPc-p framework over its molecular NiPc counterparts.

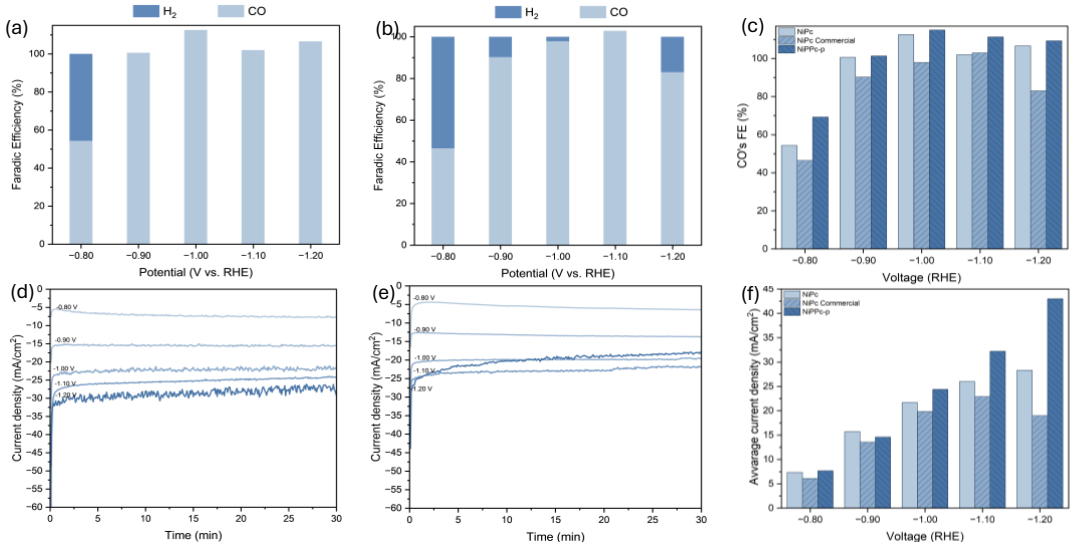


Figure 9 | CO_2RR activity and selectivity of molecular NiPc catalysts. FE of (a) synthesized NiPc and (b) commercial NiPc; (c) FE comparison with NiPPc-p; chronoamperometric profiles of (d) synthesized NiPc and (e) commercial NiPc; and (f) average current-density comparison with NiPPc-p. All catalysts were evaluated at 0.4 mg cm^{-2}.

This enhanced performance of the Ni active sites within the polyphthalocyanine framework may be associated with the extended π-conjugated structure of the polymer, which has been reported to facilitate electron delocalization and charge transport throughout the framework [14]. Compared with previously reported Ni-phthalocyanine-based catalysts for CO_2-to-CO conversion, NiPPc-p exhibited highly competitive performance, combining essentially quantitative CO Faradaic efficiency with high current density under H-cell conditions (Table 1).

Table 1 | Performance summary of representative Ni-phthalocyanine-based catalysts for CO_2RR to CO in H-type cells with 0.5 M $KHCO_3$ electrolyte.

Catalyst	j (mA cm^{-2})	FE % (CO)
NiPc-OMe-MDE [17]	14.5	100
NiPcTs/CB [19]	4.9	95
$Ni(NH_2)_8$Pc-GC [20]	17.6	95
NiTAPc/CNT [21]	16.7	100
3D-NiPc-COF [22]	13.97	90
NiPc-THB [23]	27.99	92.3
NiPc-TFPN COF [24]	14.1	99.8
NiPPc-p [This work]	43	100

Conclusion

In summary, Ni and Co-Ni-based polyphthalocyanines were developed to regulate the reduction pathways and selectivity of electrochemical CO_2 reduction. The bimetallic Co-Ni systems exhibited composition-dependent reduction pathways, with $Co_{3-1}Ni_1$PPc enabling deeper CO_2 reduction toward methanol. More significantly, modification of the Ni polyphthalocyanine with TPPA capping agent produced NiPPc-p, which achieved essentially 100% CO Faradaic efficiency from -0.90 to -1.20 V versus RHE with no detectable H_2 formation while reaching an average current density of approximately 43 mA cm^{-2} at -1.20 V versus RHE in H-type cell electrolysis. Optimisation of the catalyst loading identified 0.4 mg cm^{-2} as providing the most favourable current density and stability. NiPPc-p further outperformed molecular NiPc in selectivity, current response, and electrochemical stability, demonstrating the beneficial role of the conjugated polymeric framework in enhancing the performance of the Ni active sites. These findings establish framework and edge modification of polyphthalocyanines as an effective strategy for directing CO_2 reduction pathways and achieving highly selective CO_2-to-CO electrocatalysis. Future work will focus on extending NiPPc-p to flow-cell systems, where improved CO_2 mass transport could enable higher current densities and larger-scale electrolysis, together with further characterization to better understand its enhanced catalytic performance.

References

1. Belsa, B. et al. Materials challenges on the path to gigatonne CO_2 electrolysis. Nat. Rev. Mater. 9, 535–549 (2024). https://doi.org/10.1038/s41578-024-00696-9

2. Elokl, M. A. et al. Integrated CO_2 capture and conversion: dual-functional materials, mechanisms, and pathways to industrial decarbonization. EES Catal. 4, 522–641 (2026). https://doi.org/10.1039/D5EY00322A

3. Faust, M. et al. Carbon monoxide separation: past, present and future. Chem. Soc. Rev. 52, 4691–4736 (2023). https://doi.org/10.1039/D3CS00147D

4. Hutchison, P. et al. Proton-coupled electron transfer mechanisms for CO_2 reduction to methanol catalyzed by surface-immobilized cobalt phthalocyanine. J. Am. Chem. Soc. 146, 20230–20240 (2024). https://doi.org/10.1021/jacs.4c05444

5. Xu, C., Hong, P., Dong, Y., Robert, M., Shao, G. & Lei, Y. Toward complete CO_2 electroconversion: status, challenges, and perspectives. Adv. Energy Mater. 15, 2406146 (2025) https://doi.org/10.1002/aenm.202406146

6. She, X., Wang, Y., Xu, H., Tsang, S. C. E. & Lau, S. P. Challenges and opportunities in electrocatalytic CO_2 reduction to chemicals and fuels. Angew. Chem. Int. Ed. 61, e202211396 (2022). https://doi.org/10.1002/anie.202211396

7. Serafini, M., Mariani, F., Basile, F., Scavetta, E. & Tonelli, D. From traditional to new benchmark catalysts for CO_2 electroreduction. Nanomaterials 13, 1723 (2023). https://doi.org/10.3390/nano13111723

8. Zia, J., Radhakrishnan, S., Tejaswini, M. S. S. R. & Riaz, U. Earth-abundant metal catalysts for sustainable CO_2 reduction: a review of strategies and progress. Sustain. Energy Fuels 10, 1208–1233 (2026).

https://doi.org/10.1039/D5SE01290B

9. Li, J. et al. Molecular-scale CO spillover on a dual-site electrocatalyst enhances methanol production from CO_2 reduction. Nat. Nanotechnol. (2025). https://doi.org/10.1038/s41565-025-01866-8

10. Hassan, A., Dar, M. & Dar, M. A. Driving CO_2 conversion to C_1 and C_2 products on single-atom catalysts: recent experimental and theoretical insights. ACS Appl. Mater. Interfaces 17, 53056–53080 (2025). https://doi.org/10.1021/acsami.5c11447

11. Yang, Z.-W., Chen, J.-M., Qiu, L.-Q., Xie, W.-J. & He, L.-N. Molecular engineering of metal complexes for electrocatalytic carbon dioxide reduction: from adjustment of intrinsic activity to molecular immobilization. Angew. Chem. Int. Ed. 61, e202205301 (2022). https://doi.org/10.1002/anie.202205301

12. Li, Z. et al. A mechanism review of metal phthalocyanines as single-atomic catalysts in electrochemical energy conversion. Chem. Sci. 16, 14019–14037 (2025). https://doi.org/10.1039/D5SC03210E

13. Wang, X. et al. Two-dimensional metallophthalocyanine nanomaterials for electrocatalytic energy conversion. Energy Environ. Mater. 7, e12709 (2024). https://doi.org/10.1002/eem2.12709

14. Zhou, Y., Duan, R., Liu, L., Ding, C. & Li, C. Electrocatalytic synthesis of methylamine from nitrate and carbon dioxide on a heterometallic polyphthalocyanine. Chem. Sci. 16, 17148–17155 (2025). https://doi.org/10.1039/D5SC04641F

15. Jin, H. et al. Carbonyl-linked cobalt polyphthalocyanines as high-selectivity catalyst for electrochemical CO_2 reduction. Chem. Commun. 60, 1715–1718 (2024). https://doi.org/10.1039/D3CC05844A

16. Chen, K. et al. Nickel polyphthalocyanine with electronic localization at the nickel site for enhanced CO_2 reduction reaction. Appl. Catal. B Environ. 306, 121093 (2022). https://doi.org/10.1016/j.apcatb.2022.121093

17. Zhang, X. et al. Molecular engineering of dispersed nickel phthalocyanines on carbon nanotubes for selective CO_2 reduction. Nat. Energy 5, 684–692 (2020). https://doi.org/10.1038/s41560-020-0667-9

18. Yang, S., Yu, Y., Dou, M., Zhang, Z. & Wang, F. Edge-functionalized polyphthalocyanine networks with high oxygen reduction reaction activity. J. Am. Chem. Soc. 142, 17524–17530 (2020). https://doi.org/10.1021/jacs.0c07249

19. Zhang, X. et al. Water-soluble metal phthalocyanines enable molecularly dispersed heterogeneous electrochemical CO_2 conversion. Adv. Sci. 13, e21145 (2026). https://doi.org/10.1002/advs.202521145

20. Han, J. et al. Graphite conjugated nickel phthalocyanine for efficient CO_2 electroreduction and Zn–CO_2 batteries. Chem. Sci. 15, 15670–15678 (2024). https://doi.org/10.1039/D4SC02682A

21. Chen, S. et al. Ligand engineering in nickel phthalocyanine to boost the electrocatalytic reduction of CO_2. Adv. Funct. Mater. 32, 2111322 (2022). https://doi.org/10.1002/adfm.202111322

22. Zhang, Q., Han, B., Jin, Y., Li, M., Zhang, E. & Jiang, J. 2D and 3D phthalocyanine covalent organic frameworks for electrocatalytic carbon dioxide reduction. Chin. Chem. Lett. 36, 110330 (2025). https://doi.org/10.1016/j.cclet.2024.110330

23. Zhang, Y. et al. Single-point linkage engineering in conjugated phthalocyanine-based covalent organic frameworks for electrochemical CO_2 reduction. Nano-Micro Lett. 17, 252 (2025). https://doi.org/10.1007/s40820-025-01754-9

24. Lu, M. et al. Stable dioxin-linked metallophthalocyanine covalent organic frameworks (COFs) as photo-coupled electrocatalysts for CO_2 reduction. Angew. Chem. Int. Ed. 60, 4864–4871 (2021). https://doi.org/10.1002/anie.202011722